15th IFK
Proc. of the 15th International Fluid Power Conference <Symposium/Conference>
<DOI>

Energy efficiency evaluation of hybrid distributed-centralized load sensing system for electrified excavator

Hongyun Mu[a], Min Cheng[a,*], Xiongfeng Tang[a]

a State Key Laboratory of Mechanical Transmission for Advanced Equipment, Chongqing University, Chongqing 400044, China

Abstract. A hybrid distributed-centralized load sensing (HDC-LS) system is a potential solution for reducing energy consumption in electric construction machinery. It balances load differences by establishing a hybrid distributed-centralized actuator (HDCA) through the parallel connection of a distributed actuator alongside the original hydraulic cylinder. The characteristic of the excavator actuator, which is highly involved in compound motions, is exploited to equip the arm with the HDCA in this study. A parameter design approach is proposed that fully considers multiple HDCA factors, including load balance capacity, nominal power, and installation space. Compared with the conventional EHA, the integrated HDCA reduces the volume and mass by 43.9% and 27.3%, respectively, for a nominal power of 5 kW. Simulation results for a 6 T electrified excavator show that battery energy consumption is reduced by 2.2% – 15.6% for HDCA nominal powers of 3 – 7 kW, compared with the conventional load sensing (LS) system.

Keywords. Electric excavator, Load sensing, Load differences, Integrated, Installation space, Energy efficiency evaluation.

1. INTRODUCTION

With the international community increasingly focusing on policies of carbon neutrality and carbon peaking, the development of new, highly efficient construction machinery has become more urgent in recent years [1]. The load sensing (LS) system matchs pressure by controlling the pump outlet pressure to be one pressure margin higher than the load pressure. Offering advantages such as simple and reliable operation control, it is widely used in small and medium-sized excavators. However, the system exhibits substantial energy losses that originate from two dominant mechanisms.

(1) Control valve losses. These losses are termed meter-in (upstream) or meter-out (downstream) throttling losses, depending on their location relative to the actuator. The former can be partially reduced by variable pressure margin control, but this approach requires extra sensors and signal-conditioning electronics [2]. The latter can be addressed by potential energy recovery, but this requires additional energy-conversion components, the implementation of which is often constrained by space limitations. The independent metering control system is an effective solution for reducing these throttling losses [3]. However, the excessively low pressure differential across the valve orifice can easily trigger oscillations, resulting in poor system stability [4].

(2) Load differences loss. Previous studies have tackled this problem through four mainstream approaches. 1) The hydraulic transformers. Due to their complex structure, production costs remain high, posing significant challenges to commercialization [5]. 2) The multi-pressure sources. These systems require multiple components (e.g., pumps, accumulators, switching valves), leading to complex structures, high costs, and large space requirements [6]. 3) The multi-chamber cylinder. When the actuator load changes, frequent mode switching by the control valve is required to select a new working chamber. This results in pressure shocks and poor system controllability [7]. 4) The distributed control systems. Purely distributed systems suffer from high installed power and large installation space.

To address the issue of low energy efficiency caused by load difference, a hybrid distributed-centralized load sensing (HDC-LS) system was proposed in our previous work [8]. The results obtained from an excavator's boom showed advantages of high energy efficiency and ease of implementation. In this study, the parameter design criterion for the HDCA is further discussed to systematically consider its key factors, including load balance capacity, nominal power, and installation space. A parameter design approach is proposed for the HDCA and the control valve to make tradeoffs among nominal power, installation space, and energy-saving capacity. Furthermore, an integrated HDCA with a four-chamber hydraulic cylinder is designed and validated on a 6 T electrified excavator under different nominal powers.

2. LAYOUT OF THE HDC-LS SYSTEM

As shown in Figure 2.1, the basic mechanism of the HDC-LS system is to establish an HDCA by connecting an electro-hydrostatic actuator (EHA) (distributed actuator) in parallel alongside the original hydraulic cylinder (centralized actuator). The four-quadrant operation of the EHA is exploited to balance the load difference. When the HDCA is the highest-load actuator, the EHA applies an auxiliary force to adjust the meter-in chamber pressure down to that of the second-highest actuator, thereby reducing LS pump energy consumption. Conversely, when the HDCA is not the highest-load actuator, the EHA applies a resistive force to achieve pressure matching, thereby recovering the lost energy of the pressure compensator. Furthermore, the EHA can also recover the potential energy under overrunning loads during load balancing. The principle of the EHA controller is shown in Figure 2.1 (d), with details referenced in our previous work [8]. In this study, the case of the HDCA installed on the excavator's arm is considered to discuss a design criterion. There are three reasons as follows.

(1) The nominal power of the HDCA should be high enough to achieve full load balance and energy recovery under different conditions. The arm experiences more complex four-quadrant loads than the boom. Therefore, accurate and uniform evaluation of the load difference under compound motion is necessary.

(2) The HDCA includes many components such as an electric motor, a valve block, and a hydraulic pump. The increased mass has a significant impact on the required force and, thereby, on the energy consumption.

(3) The HDCA is sensitive to size constraints when installed on the arm of the excavator or other machinery. The HDCA should be designed carefully within limited installation space to avoid structural interference.

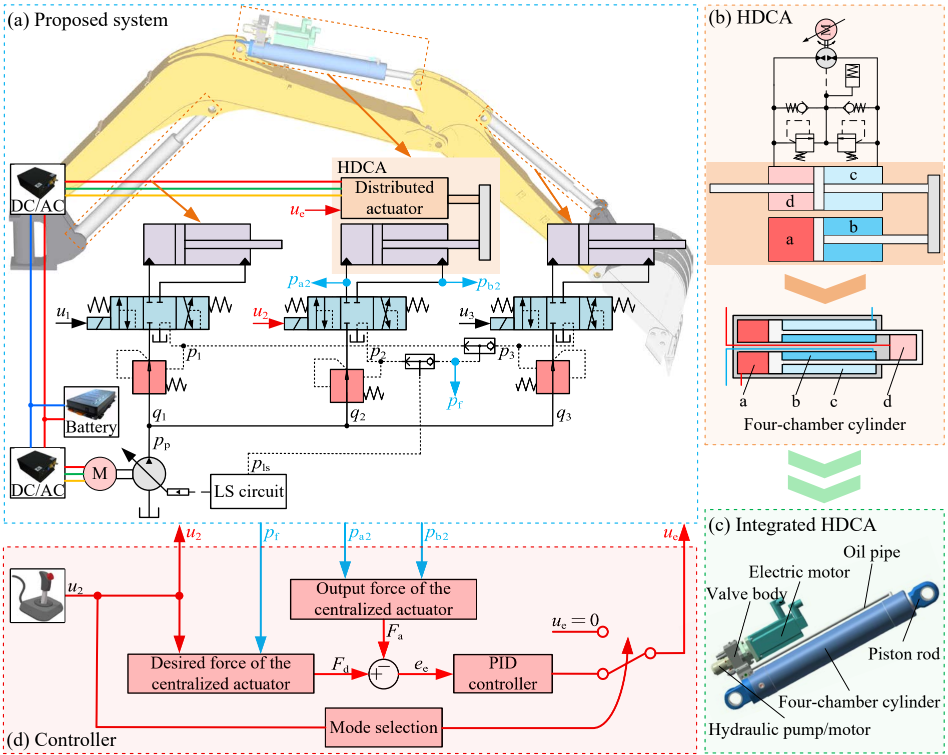

Figure 2.1. Working principle of the HDC-LS system

3. Parameter Design Approach

The flow diagram of the parameter design is shown in Figure 3.1. For the distributed actuator, the key criterion for parameter design is to identify the relationship between EHA nominal power (HDCA nominal power) and energy-saving capability. The load forces of three actuators during the excavating cycle are obtained through load characteristic modelling. The EHA output force is calculated assuming fully balanced load differences, and its probability distribution is derived. A power coverage ratio is calculated by combining the probability distribution of EHA velocity, and this ratio is used as an index for evaluating energy-saving capability. For the centralized actuator, the meter-out orifice of the control valve is redesigned based on the selected HDCA nominal power to compensate for loads exceeding the nominal power.

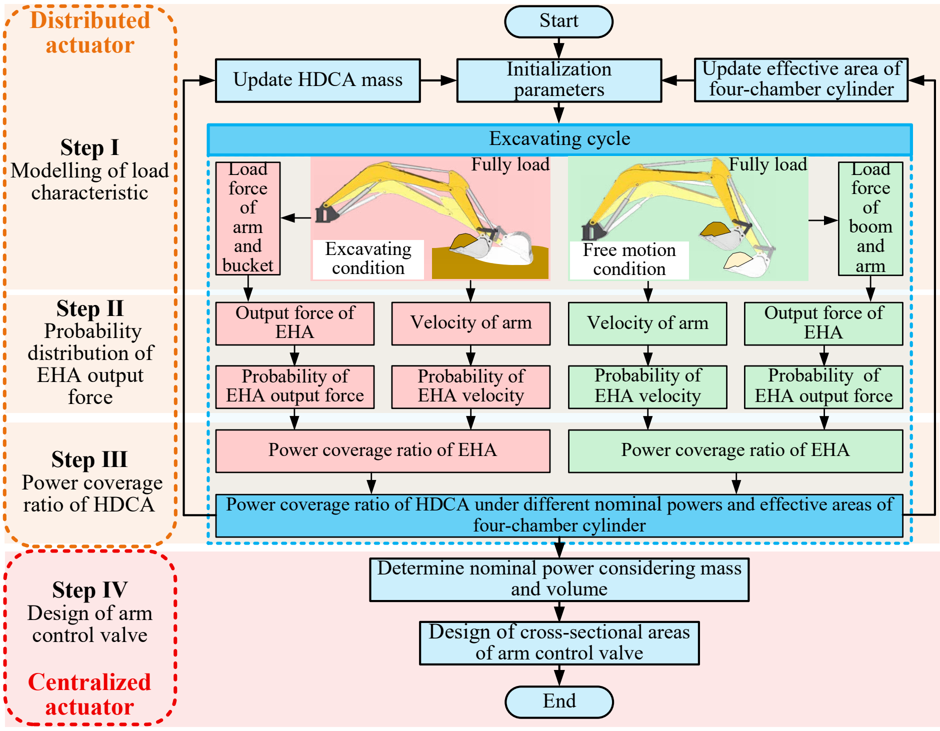

Figure 3.1. Flow diagram of the parameter design

3.1. *Distributed actuator*

3.1.1. Modelling of load characteristic

A typical excavating cycle is shown in Figure 3.2(a), which consists of four working steps: digging, lifting, dumping, and lowering. To evaluate the energy-saving capability of the HDCA, the excavating cycle is divided into two conditions: soil interaction condition (Figure 3.2(b)) and free motion condition (Figure 3.2(c)).

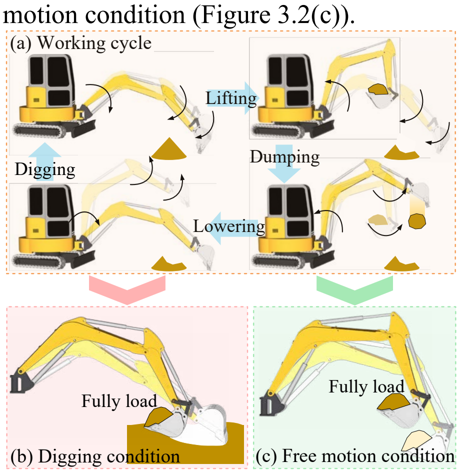

Figure 3.2. Typical excavating cycle and its two conditions

1) Full load excavating condition. The arm and bucket cylinders typically extend in a compound motion for soil excavation, while the boom has a rare or small movement. The digging force is applied to the bucket tip by the soil. Specifically, the mass of the HDCA impact on energy consumption is considered in the modelling process. Furthermore, to guarantee that the load forces represent the operating conditions of the arm and bucket cylinders across various postures, the modelling process considers different boom displacements. 2) Full load free motion condition. The boom, arm, and bucket cylinders perform a compound motion to complete the soil dumping. Similarly, the effects of different bucket displacements on the load forces are considered. During the excavating condition, static equilibrium balances the excavating force and manipulator gravity against the hydraulic cylinder output. During the free-motion condition, it balances the combined gravity of the soil and manipulator against the hydraulic cylinder output. The load force of the actuators is shown Figure 3.3.

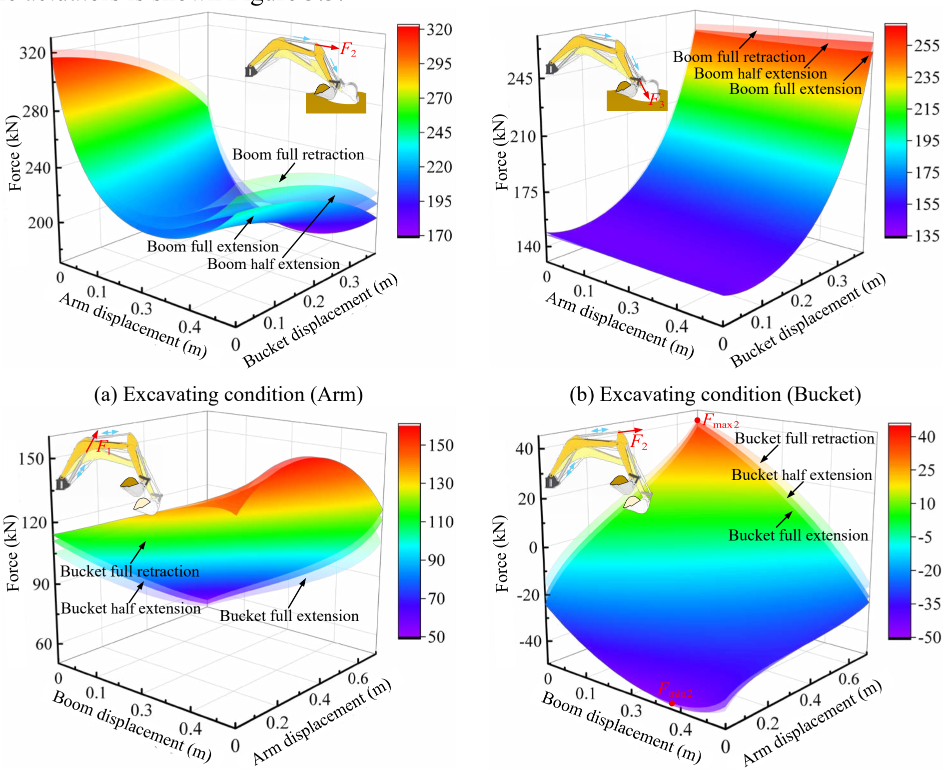

(a) Excavating condition (Arm)
(b) Excavating condition (Bucket)
(c) Free motion condition (Boom)
(d) Free motion condition (Arm)

Figure 3.3. Load forces of the actuators

3.1.2. Probability distribution of EHA output force

The four-chamber cylinder structure is shown in Figure 3.4. To ensure the digging force of the arm, the effective area A_{a2} of chamber "a" in the four-chamber cylinder of the centralized actuator must not be less than that of the original cylinder. 1) Full load excavating condition. When the excavator is in excavating condition, both the arm and bucket actuators are typically extended. Ignoring friction, the steady state force equilibrium equation for the arm and bucket can be expressed as:

$$\begin{cases} F_2 = (p_{a2}A_{a2} - p_{b2}A_{b2}) + F_{Eha} \\ F_3 = p_{a3}A_{a3} - p_{b3}A_{b3} \end{cases} \tag{3.1}$$

where F_2 and F_3 represent the load forces on the arm and bucket, respectively (positive direction is defined as cylinder extension); F_{Eha} indicates the output force of the EHA; p_{a2} and p_{b2} denote the pressure in chambers "a" and "b"; A_{b2} is the effective area in chamber "b"; p_{a3} and p_{b3} are the head-side and rod-side pressures of the bucket cylinder; and A_{a3} and A_{b3} represent the corresponding effective areas. Here, p_{b2} with the meter-out orifice fully open for potential energy recovery. p_{b3} can be derived from the orifice equation, which is:

$$q = C_d A_d \sqrt{\frac{2\Delta p}{\rho}} \tag{3.2}$$

where q represents the flow rate; C_d indicates the flow coefficient; ρ denotes the oil density; A_d is the cross-sectional area; and Δp represents the differential pressure. Therefore, p_{b2} and p_{b3} can be expressed as:

$$\begin{cases} p_{b2} = 0, \quad \text{Arm extends} \\ p_{b3} = \dfrac{\rho q_{b3}^2}{2C_d^2 A_{db3}^2}, \quad \text{Bucket extends} \end{cases} \tag{3.3}$$

where q_{b3} and A_{db3} represent the flow rate and cross-sectional area of the bucket control valve, respectively. When the EHA adjusts the load pressure of the centralized actuator so that it is consistent with the load-pressure feedback from other actuators, the load differences are fully balanced, that is:

$$p_{a2} = p_f = p_{a3} \tag{3.4}$$

where p_f represents load pressure feedback from other actuators. From Eqs. (3.1) and (3.4), F_{Eha} can be inferred as:

$$F_{Eha} = F_2 - \frac{F_3 + p_{b3}A_{b3}}{A_{a3}} A_{a2} \tag{3.5}$$

From Eq. (3.5), F_{Eha} can be calculated for different displacements of the arm and bucket, as shown in Figure 3.5. 2) Full load free motion condition. Similarly, F_{Eha} can be obtained according to the direction of motion of the boom and arm, as shown in Figure 3.6.

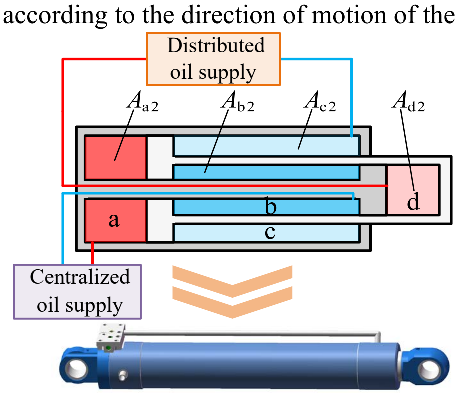

Figure 3.4. Structure of the four-chamber cylinder

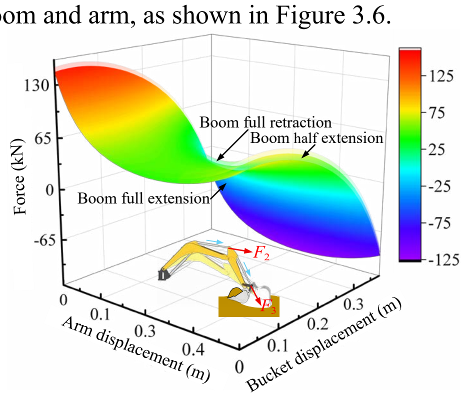

Figure 3.5. Output force of the EHA under excavating condition

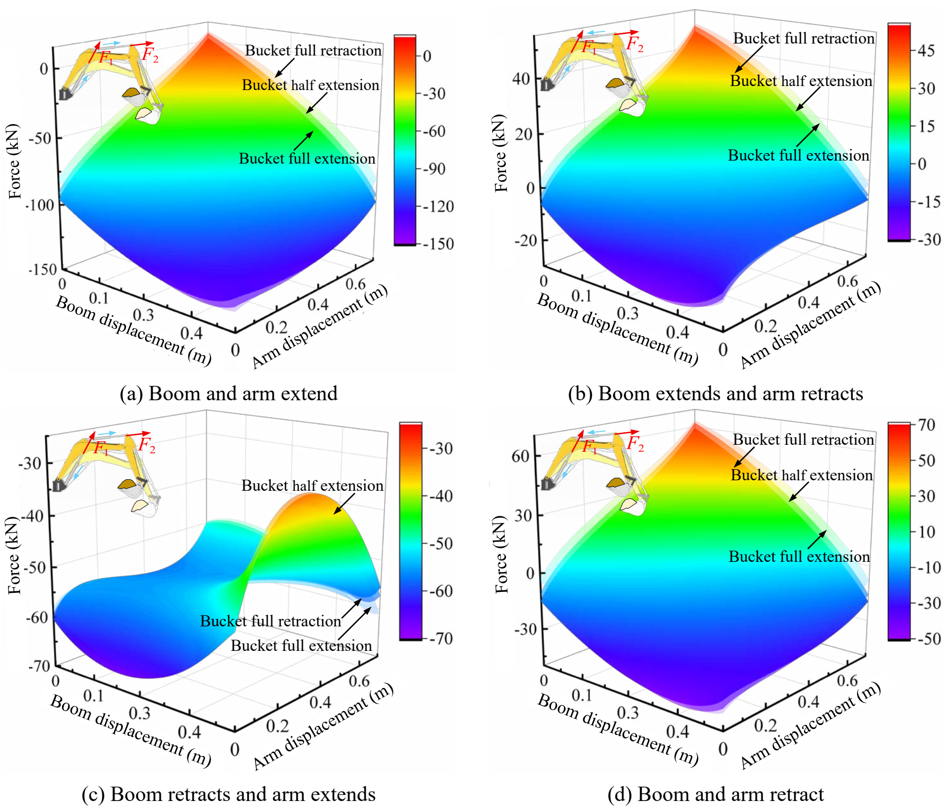

Figure 3.6. Output force of the EHA under free motion condition

3.1.3. Power coverage ratio of HDCA

As shown in Figure 3.5 and Figure 3.6, F_{Eha} is stochastic under different motion conditions. To better describe this complex load characteristic, its probability distribution is calculated for the typical excavating cycle by uniformly segmenting F_{Eha} several zones. The probability distribution and segmenting can be expressed as:

$$\begin{cases} \begin{cases} P_{\mathrm{FDig}} = \dfrac{n_i}{n_{11}} \cdot 100\%, \\ F_{\mathrm{D1}} + \dfrac{F_{\mathrm{U1}} - F_{\mathrm{D1}}}{z_1}(i-1) \le F_{\mathrm{Eha}} < F_{\mathrm{D1}} + \dfrac{F_{\mathrm{U1}} - F_{\mathrm{D1}}}{z_1} i, \end{cases} i = 1,2,3,\dots,z_1 \quad \text{Excavating condition} \\ \begin{cases} P_{\mathrm{FFre}} = \dfrac{n_j}{n_{21}+n_{22}+n_{23}+n_{24}} \cdot 100\%, \\ F_{\mathrm{D2}} + \dfrac{F_{\mathrm{U2}} - F_{\mathrm{D2}}}{z_2}(j-1) \le F_{\mathrm{Eha}} < F_{\mathrm{D2}} + \dfrac{F_{\mathrm{U2}} - F_{\mathrm{D2}}}{z_2} j, \end{cases} j = 1,2,3,\dots,z_2 \quad \text{Free motion condition} \end{cases} \tag{3.6}$$

where P_{FDig} and P_{FFre} represent the probabilities within the output force of segment i and j, respectively; F_{U1}, F_{D1}, F_{U2} and F_{D2} indicate the upper and lower limits; z_1 and z_2 denote the number of segments; n_i and n_j are the number of sample points within each segment; and n_{11} and n_{21} represent the numbers of sample points for F_{Eha} Figure 3.5 and Figure 3.6 (each actuator displacement step corresponds to a sample point). During each motion phase, the velocities of the arm actuator typically tend toward a normal distribution. Therefore, the probability β_{v} at the velocity v_{Eha} can be expressed as:

$$\beta_{\mathrm{v}} = \frac{\mathrm{e}^{-\frac{(v_{\mathrm{Eha}}-\mu)^2}{2\sigma^2}}}{\sqrt{2\pi}\sigma} \cdot 100\% \tag{3.7}$$

where μ and σ represent the mean and standard deviation, respectively. The total number of the EHA power sample points is defined as w. In each segment, m output-force samples are calculated based on the probability distribution, and m velocity samples are generated randomly according to the velocity distribution. Considering the efficiencies η_{Pum} and η_{Cyl} of the hydraulic pump and cylinder, the power P_{Eha}^k corresponding to each sample point for the distributed side can be expressed as:

$$P_{\mathrm{Eha}}^k = \begin{cases} \dfrac{F_{\mathrm{Eha}}^k v_{\mathrm{Eha}}^k}{\eta_{\mathrm{Pum}}\eta_{\mathrm{Cyl}}}, & (F_{\mathrm{d}}^k v_{\mathrm{d}}^k \geq 0) \text{ Under resistive condition} \\ F_{\mathrm{Eha}}^k v_{\mathrm{Eha}}^k \eta_{\mathrm{Pum}}\eta_{\mathrm{Cyl}}, & (F_{\mathrm{d}}^k v_{\mathrm{d}}^k < 0) \text{ Under overrunning condition} \end{cases}, \quad k = 1,2,\cdots,w \tag{3.8}$$

where F_{Eha}^k and v_{Eha}^k represent the output force and velocity corresponding to each sample point, respectively. To achieve better load balance, a higher nominal power of the EHA is preferable to cover all P_{Eha}^k, but is limited by the installation space of the arm. To evaluate the load balance capacity, the power coverage ratio of the HDCA is introduced as an evaluation index. The schematic of the power coverage ratio under different motion conditions is shown in Figure 3.7. Here, the red and blue points represent power sample points P_{Eha}^k, and the green curve is the nominal power P_{Mot} of the EHA electric motor. P_{Eha}^k are distributed according to the joint probability distribution of the velocity and the output force of the distributed side. The light blue area represents the sufficient nominal power ($P_{\mathrm{Eha}}^k \leq P_{\mathrm{Mot}}$), while other colored areas represent the insufficient power ($P_{\mathrm{Eha}}^k > P_{\mathrm{Mot}}$). The EHA operates in two-quadrant modes during the soil interaction condition: extension condition with resistive load (ECRL) and extension condition with overrunning load (ECOL). When $P_{\mathrm{Eha}}^k > P_{\mathrm{Mot}}$ (light green and orange regions in Figure 3.7(a)), the excess power is consumed by the pressure compensator (ECRL mode: bucket compensator; ECOL mode: arm compensator). During the free motion condition, the EHA operates in four-quadrant modes: ECRL, ECOL, retraction condition with overrunning load (RCOL), and retraction condition with resistive load (RCRL). Similarly, when $P_{\mathrm{Eha}}^k > P_{\mathrm{Mot}}$ (yellow, orange, and black regions in Figure 3.7(b)), the excess power is consumed by the pressure compensator or control valve. Under ECRL and RCRL modes, it is consumed by the boom compensator. Under RCOL and ECOL modes, the arm control valve takes priority and consumes the excess power, while the arm pressure compensator compensates for the insufficient power. Therefore, the power coverage ratio P_{Cov} of the EHA can be expressed as:

$$P_{\mathrm{Cov}} = \frac{w_1}{w} \cdot 100\% \tag{3.9}$$

where w_1 presents the number of sample points ($P_{\mathrm{Eha}}^k \leq P_{\mathrm{Mot}}$). The distributions of the excavating condition and the free motion condition are determined to be 1/3 and 2/3, respectively, through statistical analysis of multiple typical excavating cycles. Therefore, the power coverage ratio P_{Cyc} of the HDCA under excavating cycle can be expressed as:

$$P_{\mathrm{Cyc}} = \frac{P_{\mathrm{CovDig}}}{3} + \frac{2P_{\mathrm{CovFre}}}{3} \tag{3.10}$$

where P_{CovDig} and P_{CovFre} represent the power coverage ratios of the EHA for the excavating condition and free motion condition, respectively.

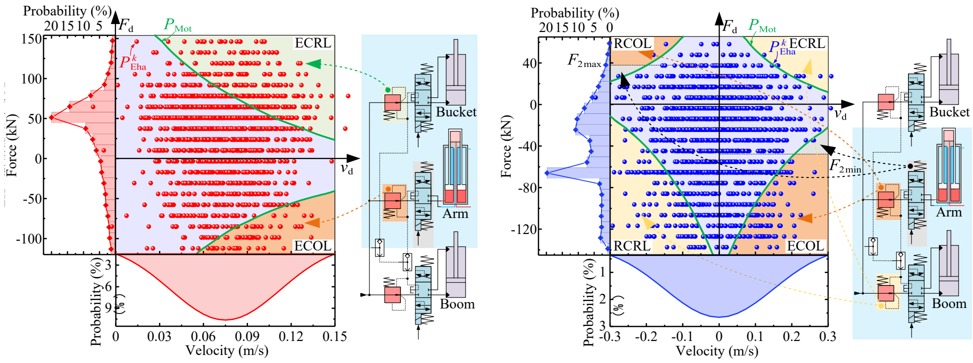

(a) Excavating condition (b) Free motion condition

Figure 3.7. Schematic of the power coverage ratio under different motion conditions

The power coverage ratio of the HDCA needs to consider the effects of its mass and the effective area of the four-chamber cylinder:

(1) HDCA mass. The mass of the HDCA can be equivalently transferred to the boom when the arm is equipped with the HDCA, as shown in Figure 3.8. Thus, the equivalent mass m_1' of the boom can be expressed as:

$$m_1' = m_1 + k_{\mathrm{L}} m_{\mathrm{Hdca}} \tag{3.11}$$

where k_{L} represents the coefficient; m_1 indicates the mass of the boom; and m_{Hdca} denotes the additional mass of the HDCA.

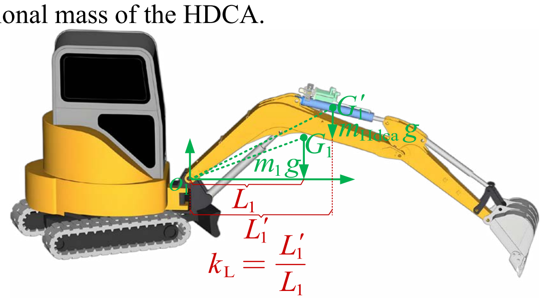

Figure 3.8. Equivalent mass of the boom

(2) Effective area of the four-chamber cylinder. To guarantee that the EHA can output maximum force within pressure limits in the EHA circuit, the effective areas A_{c2} and A_{d2} of the symmetrical chambers are selected to be half of A_{a2}.Therefore, the area coefficient k_{Are} can be described as:

$$k_{\mathrm{Are}} = \frac{2A_{\mathrm{b2}}'}{A_{\mathrm{a2}}},\quad 0 < k_{\mathrm{Are}} < 1 \tag{3.12}$$

where A_{b2}' represents the new effective area of chamber "b" in the four-chamber cylinder.

The comparison of volume and mass between HDCA and conventional EHA (arm EHA with purely distributed drive in [9]) is shown in Figure 3.9. It can be observed that the percentage decrease in volume and mass of the HDCA gradually decreases with P_{Mot}. When P_{Mot} is 5 kW, the volume and mass are reduced by 43.9% and 27.3%, respectively. By combining Eqs. (3.1) – (3.12), P_{Cyc} for different values of P_{Mot} and k_{Are} can be calculated, as shown in Figure 3.10.

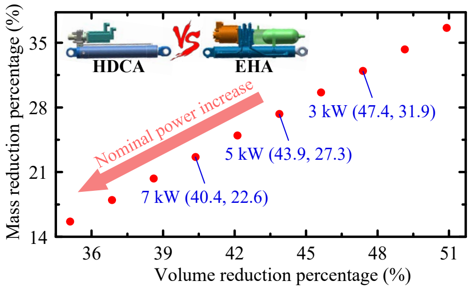

Figure 3.9. Comparison of volume and mass between HDCA and EHA

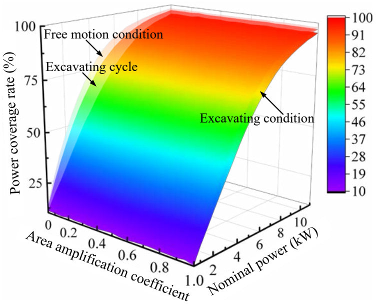

Figure 3.10. Power coverage ratio of the HDCA

3.2. Centralized actuator

When the arm is in overrunning mode, it is necessary to avoid the HDCA overspeed because of insufficient output force. Therefore, the cross-sectional area acquires to be redesigned. The energy-saving effects of the system are evaluated for $k_{\mathrm{Are}} = 0.43$ and P_{Mot} of 3 kW, 5 kW, and 7 kW. Correspondingly, P_{Cyc} is 56.8%, 76.2% and 87.3%, respectively, from Figure 3.10. Considering the limitations of the EHA components, the actual output force F_{EhaAct} can be expressed as:

$$F_{\mathrm{EhaAct}} = \min\left(\left|\frac{P_{\mathrm{Mot}}}{v_{\mathrm{Eha}}\eta_{\mathrm{Pum}}\eta_{\mathrm{Cyl}}}\right|, F_{\mathrm{Com}}\right), \quad \text{EHA under overrunning condition} \tag{3.13}$$

where F_{Com} represents the maximum output force limited by the EHA components. The back pressure p_{Bac1} and p_{Bac2} required at the control valve can be expressed as:

$$\begin{cases} p_{\mathrm{Bac1}} = \max\left(p_s, \dfrac{F_{\mathrm{Min2}} - F_{\mathrm{EhaAct}}}{A_{\mathrm{b2}}}\right), & \text{Arm extends} \\ p_{\mathrm{Bac2}} = \max\left(p_s, \dfrac{F_{\mathrm{Max2}} - F_{\mathrm{EhaAct}}}{A_{\mathrm{a2}}}\right), & \text{Arm retracts} \end{cases} \tag{3.14}$$

where F_{Min2} and F_{Max2} represent the maximum gravitational forces that the EHA needs to overcome in overrunning mode (shown in Figure 3.3(d)); and p_s indicates the minimum pressure to guarantee control performance. The flow rate q_{Bac1} and q_{Bac2} of the control valve can be expressed as:

$$\begin{cases} q_{\mathrm{Bac1}} = A_{\mathrm{b2}} v_2, & \text{Arm extends} \\ q_{\mathrm{Bac2}} = A_{\mathrm{a2}} v_2, & \text{Arm retracts} \end{cases} \tag{3.15}$$

Here, v_{Eha} can be expressed through the control valve opening k_{Ope} as follows:

$$v_{\mathrm{Eha}} = k_{\mathrm{Ope}} v_{\mathrm{Max2}} \tag{3.16}$$

where v_{Max2} represents the maximum velocity of the arm. From Eq. (3.2), the designed cross-sectional area A_{d1} and A_{d2} can be calculated using the flow formula as follows:

$$\begin{cases} A_{\mathrm{d1}} = \dfrac{q_{\mathrm{Bac1}}}{C_d\sqrt{\frac{2(p_{\mathrm{Bac1}} - p_{\mathrm{T}})}{\rho}}}, & \text{Arm extends} \\ A_{\mathrm{d2}} = \dfrac{q_{\mathrm{Bac2}}}{C_d\sqrt{\frac{2(p_{\mathrm{Bac2}} - p_{\mathrm{T}})}{\rho}}}, & \text{Arm retracts} \end{cases} \tag{3.17}$$

where p_{T} represents the tank pressure ($p_{\mathrm{T}} = 0$). From Eqs. (3.13) – (3.17), A_{d1} and A_{d2} (blue curve) for different k_{Ope} values are obtained when P_{Mot} is 3 kW, 5 kW, and 7 kW, respectively, as shown in Figure 3.11. To reduce the difficulty of valve machining, A_{d1} and

A_{d2} are modified to obtain a smooth and monotonically increasing design curve (green curve).

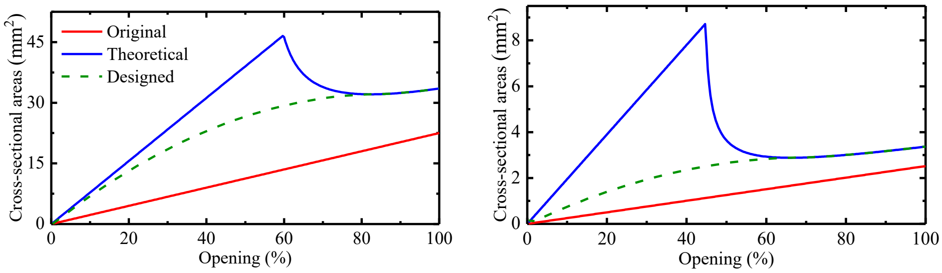

(a) Arm retracts (b) Arm extends

Figure 3.11. Cross-sectional area of the arm control valve (5 kW)

4. Simulation study

4.1. *Simulation modelling*

A 6 T electric excavator driven by a conventional LS system is taken as the reference prototype. A simulation model of this prototype is built in the AMESim environment. Based on the simulation model, the arm cylinder is replaced with an HDCA to establish the HDC-LS system. The models are simulated under the same excavation cycle to evaluate the energy-saving effects and the velocity performance at HDCA nominal powers of 3 kW, 5 kW, and 7 kW.

4.2. *Comparative analysis*

4.2.1. *Motion performance*

As shown in Figure 4.1(a), the HDCA enters the extend mode and the retract mode according to the arm control signal during a typical excavation cycle. As shown in Figure 4.1(b), during the entire motion process, the arm actuator maintains nearly identical velocities with smooth dynamic speed variations because the flow control method of the conventional LS system is retained. Therefore, the designed cross-sectional area of the control valve avoids overspeed dropping caused by insufficient HDCA nominal power. This guarantees the consistent motion profiles and evaluation accuracy of energy efficiency.

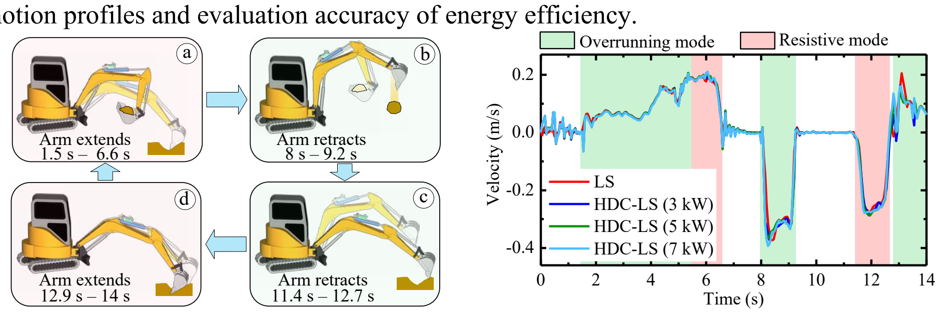

(a) Typical excavating cycle of the excavator (b) Arm

Figure 4.1. Excavating cycle and actuator velocities

4.2.2. Energy consumption performance

As shown in Figure 4.2, by controlling the EHA output force to adjust the pressures in chambers a and b of the four-chamber cylinder, the pressure differential and the energy losses across the pressure compensators are reduced. The output energy of the LS pump is reduced effectively since the EHA outputs an auxiliary force. When the EHA outputs a resistive force, it prioritizes recovering potential energy while balancing load difference.

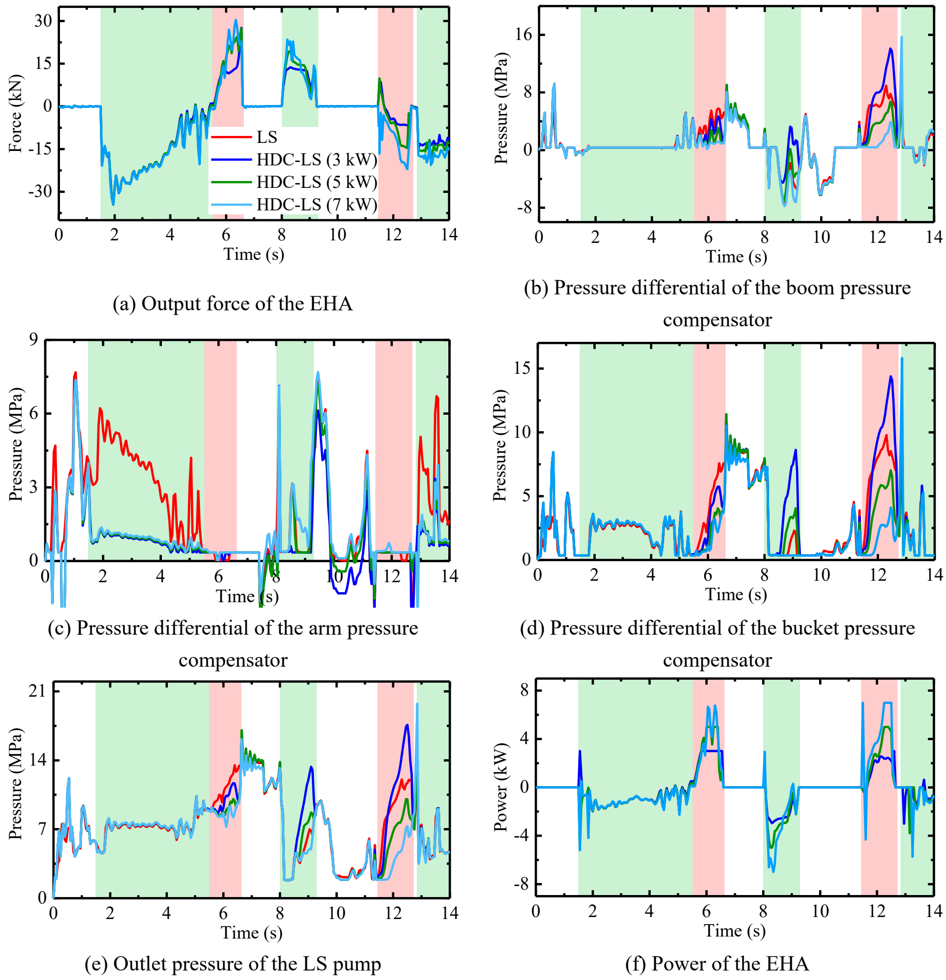

Figure 4.2. Simulation results of the conventional LS and HDC-LS systems

The system efficiency can be calculated as:

$$\begin{cases} \eta_{\mathrm{C}} = \dfrac{E_{\mathrm{Ct}} - E_{\mathrm{Cp}}}{E_{\mathrm{ct}}} \cdot 100\% \\ \eta_{\mathrm{P}} = \dfrac{E_{\mathrm{Pt}} - E_{\mathrm{Pp}}}{E_{\mathrm{Pt}}} \cdot 100\% \\ \eta_{\mathrm{S}} = \dfrac{E_{\mathrm{T}} - E_{\mathrm{P}}}{E_{\mathrm{T}}} \cdot 100\% \end{cases} \tag{4.1}$$

where η_C and η_P represent energy-saving efficiency of the pressure compensator and LS pump, respectively; η_S indicates the energy-saving efficiency; E_{Ct}, E_{Pt} and E_T denote the energy consumption of the pressure compensator, LS pump, and battery in the conventional LS system; and E_{Cp}, E_{Pp} and E_P are the energy consumption of the pressure compensator, LS pump, and battery in the HDC-LS system. Based on Eq. (4.1) and combined Figure 4.3, the system efficiencies for different HDCA nominal powers are calculated in Table 1. It can be observed that both the energy loss in the pressure compensator due to the load difference and the output energy by the LS pump are significantly reduced. As the nominal power of the HDCA increases, the load difference effect of the EHA becomes more pronounced, leading to increasing energy savings. At nominal powers of 3 kW, 5 kW, and 7 kW, the energy consumption of the battery is reduced by 2.2 %, 11.2 %, and 15.6 %, respectively.

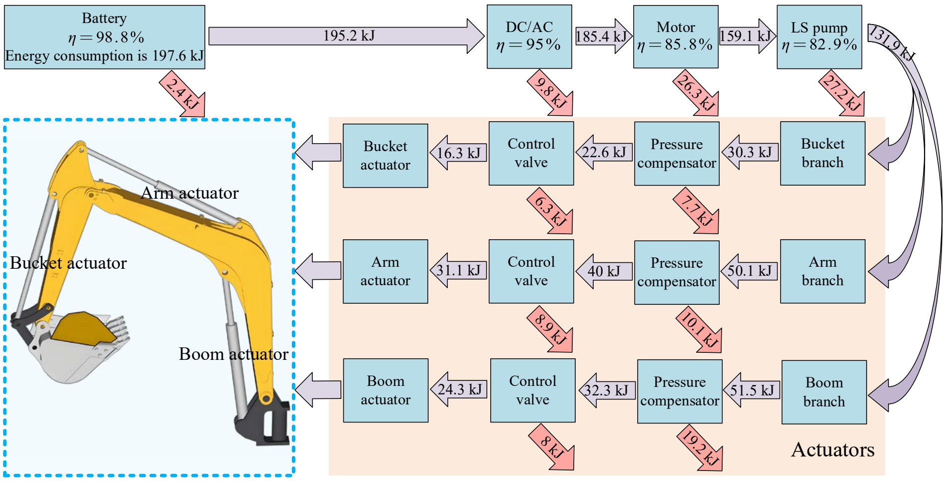

(a) LS system

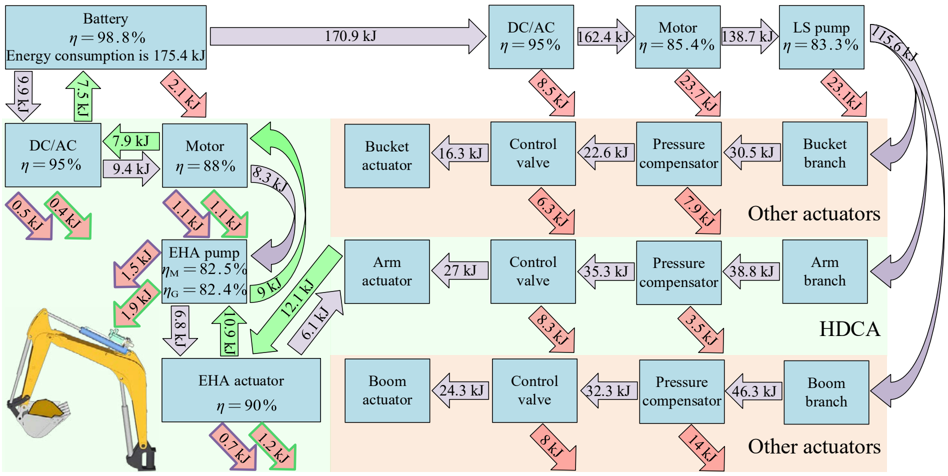

(b) HDC-LS system (5 kW)

Figure 4.3. Comparison of the energy flow for different layouts

Table 1 System efficiency for different HDCA nominal powers

Name	LS system	HDC-LS system (3 kW)	HDC-LS system (5 kW)	HDC-LS system (7 kW)
$E_{\mathrm{Ct}}/E_{\mathrm{Cp}}$	37 kJ (Boom 19.2 kJ) (Arm 10.1 kJ) (Bucket 7.7 kJ)	33.9 kJ (Boom 19.7 kJ) (Arm 3 kJ) (Bucket 11.2 kJ)	25.4 kJ (Boom 14 kJ) (Arm 3.5 kJ) (Bucket 7.9 kJ)	21.5 kJ (Boom 10.4 kJ) (Arm 4.1 kJ) (Bucket 7 kJ)
$E_{\mathrm{Pt}}/E_{\mathrm{Pp}}$	131.9 kJ	128.6 kJ	115.6 kJ	108.8 kJ
$E_{\mathrm{T}}/E_{\mathrm{P}}$	197.6 kJ	193.2 kJ	175.4 kJ	166.8 kJ
η_{C}	—	8.4%	31.4%	41.9%
η_{P}	—	2.5%	12.4%	17.5%
η_{S}	—	2.2%	11.2%	15.6%

5. CONCLUSION

In this study, a parameter design approach suitable for the HDCA when installed on the arm of electric excavator is proposed. Furthermore, the HDCA is designed to achieve an integrated drive. Compared with the conventional EHA, the integrated HDCA reduces the volume and mass by 43.9% and 27.3%, respectively, for a nominal power of 5 kW. A 6 T electric excavator simulation model of the HDC-LS system is established. The energy-saving effects of the HDC-LS system are evaluated under HDCA nominal powers of 3 kW, 5 kW, and 7 kW. The energy losses of the pressure compensator (boom + arm + bucket) are reduced by 8.4%, 31.4%, and 41.9%, respectively, through the EHA load balancing effect. This approach reduces battery energy consumption by 2.2%, 11.2%, and 15.6%. With the increase in HDCA nominal power, the energy-saving effect of the proposed system becomes increasingly significant.

6. REFERENCES

[1] T. Do, T. Dang, T. Dinh, K. Ahn, ‘Developments in energy regeneration technologies for hydraulic excavators: a review’, *Renew Sustain Energy Rev*, vol. 145, p. 111076, 2021.

[2] T. Lin, Y. Lin, H. Ren, H. Chen, Z. Li, Q. Chen, ‘A double variable control load sensing system for electric hydraulic excavator’, *Energy*, vol. 223, p. 119999, 2021.

[3] J. Chen, H. Jiang, X. Kong, C. Ai, ‘Mode switching control of independent metering fluid power systems’, *ISA Trans.*, vol. 158, pp. 735–748, 2025.

[4] L. Bachmann, J. Liu, J. Weber, “Investigation of the temperature influence on electrohydraulic valve control and presentation of a novel compensation approach for independent metering valve systems,” in *Proc. ASME/BATH 2023 Symp. Fluid Power Motion Control*, Sarasota, FL, USA, p. V001T01A031, 2023.

[5] D. Fassbender, V. Zakharov, T. Minav, ‘Utilization of electric prime movers in hydraulic heavy-duty mobile-machine implement systems’, *Autom. Constr.*, vol. 132, p. 103964, 2021.

[6] M. Huova, M. Linjama, ‘Energy efficient throttling control of a multi-pressure system using a genetic algorithm and model predictive control’, *Proc. Inst. Mech. Eng. Part I: J. Syst. Control Eng.*, vol. 236, pp. 406–417, 2022.

[7] H. Bartlett, ‘A symmetric multichamber hydraulic cylinder with variable piston area: An approach to compact and efficient electrohydrostatic actuation’, *J. Mech. Des.*, vol. 143, p. 083501, 2021.

[8] H. Mu, M. Cheng, X. Tang, R. Ding, W. Ma, 'A hybrid distributed-centralized load sensing system for efficiency improvement of electrified construction machinery', *Energy*, vol. 314, p. 134123, 2025.
[9] R. Ding, Y. Jiang, F. Yang, L. Peng, Z. Liu, W. Ma, 'Design and energy consumption analysis of a decentralized independent electro-hydraulic control system', *Ain Shams Eng. J.*, vol. 16, p. 103759, 2025.

Biographies

Hongyun Mu was born in Zunyi, China, in 1996. He received the B.S. and M.S. degrees in mechanical engineering from Guizhou University, Guiyang, China, in 2019 and 2023, respectively. He has been working toward the Ph.D. degree in mechanical engineering with State Key Laboratory of Mechanical Transmission for Advanced Equipment, Chongqing University, Chongqing, China. His research interests include electro-hydraulic control system and energy-saving technology of mobile machinery.

Min Cheng was born in Jingzhou, China, in 1987. He received the B.S. and Ph.D. degrees in mechatronics from Zhejiang University, Hangzhou, China, in 2009 and 2015, respectively. He is currently an Associate Professor with the State Key Laboratory of Mechanical Transmissions, Chongqing University, Chongqing, China. His research interests include electro-hydraulic control systems of mobile machinery, energy saving and motion control of hydraulic systems, and mechatronic systems design.

Xiongfeng Tang was born in Yiyang, China, in 2002. He received the B.S. degree in mechatronic engineering from Chongqing University, Chongqing, China, in 2023. He has been working toward the M.S. degree in mechanical engineering with State Key Laboratory of Mechanical Transmission for Advanced Equipment, Chongqing University, Chongqing, China. His research interests include high-performance electro-hydraulic transmission and control.